ELSEVIER

Journal of Nuclear Materials 283–287 (2000) 244–248

journal of nuclear materials

www.elsevier.nl/locate/jnucmat

Radiation-induced segregation in model alloys

T. Ezawa [a,*], E. Wakai [b], R. Oshima [c]

[a] *Faculty of System Engineering, University of East Asia, 2-1 Ichinomiya-gakuencho, Shimonoseki 751-8503, Japan*
[b] *Japan Atomic Energy Research Institute, Tokai-mura, Japan*
[c] *RIAST, Osaka Prefecture University, 1-2 Gakuen-cho, Sakai-city, Osaka 593, Japan*

Abstract

The dependence of the size factor of solutes on radiation-induced segregation (RIS) was studied. Ni–Si, Ni–Co, Ni–Cu, Ni–Mn, Ni–Pd, and Ni–Nb binary solid solution alloys were irradiated with electrons in a high voltage electron microscope at the same irradiation conditions. A focused beam and a grain boundary were utilized to generate a flow of point defects to cause RIS. From the concentration profile obtained by an energy dispersive X-ray analysis, the amount of RIS was calculated. The amount of RIS decreased as the size of the solute increased up to about 10%. However, as the size increased further, the amount of RIS increased. This result shows that RIS is not simply determined by the size effect rule.

1. Introduction

For alloys under irradiation, segregation of the constituent atoms is one of the important problems. One of the causes of segregation is the flow of point defects introduced by irradiation. In order to obtain a knowledge of the mechanism of RIS [1–4], simplified and systematic experiments are desired, starting with the binary solid solution alloys. Moreover, electron beam irradiation can introduce simple point defects for this purpose [5]. In this paper, six kinds of Ni binary solid solution alloys were studied by high voltage electron microscopy. Advantages of the high voltage electron microscopy are the electron irradiation and the utilization of a focused beam that generates a point defect flow in the foil plane direction. The purpose is to examine the dependence of RIS on the size of solute atoms.

2. Experimental procedure

Ni–9.0 at.% Si, Ni–5.0 at.% Co, Ni–4.9 at.% Cu, Ni–4.6 at.% Mn, Ni–5.4 at.% Pd, and Ni–2.3 at.% Nb alloys were prepared from high purity metals by melting in an induction furnace in vacuum. The foil samples were prepared for the electron microscopy. Irradiation and observation were done with 2 MeV electrons in a high-voltage electron microscope, HU-2000. After irradiation, the irradiated region was analyzed by an energy dispersive X-ray analyzer, EDX, in a 200 kV STEM, H-800. The probe beam size was from 15 to 20 nm in diameter. The concentration was calculated by the Cliff–Lorimer method [6]. Four times the standard deviation is used as the length of the error bars in the figures presented here.

3. Results

Damage structures by some irradiation temperatures in the Ni–Cu alloy are shown in Figs. 1(a)–(f). For stabilized temperature control and minimum dislocation loop production, irradiations were performed at 773 K. Figs. 1(a)–(f) show regions irradiated and, the results of analyzing the region are shown in Figs. 2(a)–(f), respectively. Samples were analyzed along the diameter of the beam with the equal foil thickness. A focused irradiation beam with a Gausian shape was used for Figs. 1(e) and 2(e), while an unfocused beam was used for Figs. 1(d) and 2(d). Since Fig. 2(e) showed clearer concentration-change than Fig. 2(d), the focused beam

* Corresponding author. Tel.: +81-832 56 1111; fax: +81-832 56 9577.
E-mail address: ezawa@po.pios.cc.toua-u.ac.jp (T. Ezawa).

0022-3115/00/$ - see front matter
PII: S0022-3115(00)00343-3

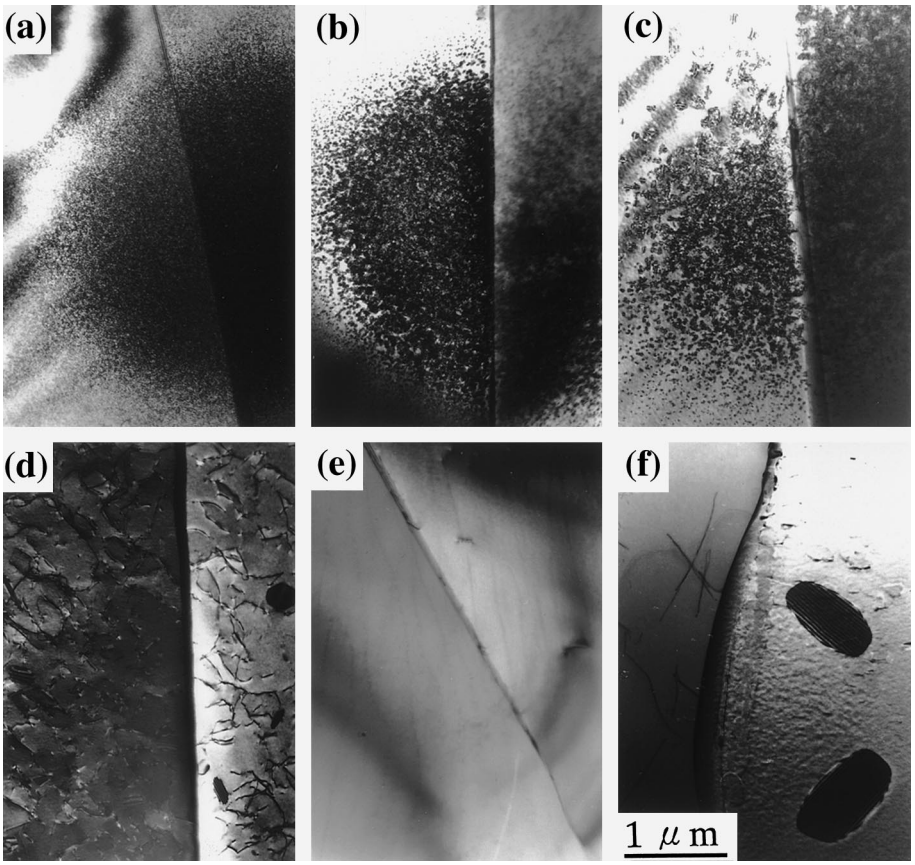

Fig. 1. Electorn micrographs of Ni–Cu alloys irradiated with 2 MeV electrons at various temperatrues. Irradiation conditions are: (a) 1.0×10^{24} e^-/m^2 s for 600 s at 373 K; (b) 1.0×10^{24} e^-/m^2 s for 600 s at 473 K; (c) 5.4×10^{23} e^-/m^2 s for 732 s at 573 K; (d) 2.3×10^{23} e^-/m^2 s for 600 s at 673 K; (e) 2.2×10^{24} e^-/m^2 s for 600 s at 673 K; (f) 5.4×10^{23} e^-/m^2 s for 732 s at 773 K, respectively. A grain boundary existed across the beam center in each sample.

was chosen, and the irradiation condition was decided as 5.4×10^{23} e^-/m^2 s for 732 s. This value was chosen for maintaining stabilized beam shape. In the figures, bars under the profiles indicate FWHM of the beam. Damage structures in a grain and in the region with a grain boundary irradiated with the focused beam in Ni–Mn alloys are shown in Figs. 3(a) and (b), respectively. Results of analysis of the region of Fig. 3 are shown in Fig. 4. Although there is a lowering of the Mn concentration in the grain boundary in Fig. 4(b), the clear concentration-change is not found in Fig. 4(a). Therefore, in the following, the region including a grain boundary is irradiated with the focused beam under the above-mentioned irradiation conditions. Electron micrographs of irradiated Ni–Si, Ni–Co, Ni–Pd, and Ni–Nb are shown in Figs. 5(a)–(d). The micrographs of Ni–Cu and Ni–Mn irradiated with the same irradiation condition are already shown in Figs. 1(f) and 3(b), respectively. The dislocation structure develops in Ni–Si, Ni–Mn, Ni–Pd and Ni–Nb, as shown in Fig. 5. In these regions, voids were observed in Ni–Mn, Ni–Pd and Ni–Nb. The void density, the average size of voids and the swelling in Ni–Mn, Ni–Pd, and Ni–Nb are 3.5×10^{20} m^{-3}, 11 nm, 4.7×10^{-2}%, 4.1×10^{20} m^{-3}, 24 nm, 5.8×10^{-1}%, 3.5×10^{20} m^{-3}, 17 nm, 1.9×10^{-1}%, respectively. In Figs. 6(a), (b), (c) and (d), results of the analysis of regions of Figs. 5(a), (b), (c) and (d) are, respectively, shown. Results of analysis of Ni–Cu and Ni–Mn are already shown in Figs. 2(f) and 4(b), respectively. In order to obtain more distinct profiles of Ni–Mn, Ni–Pd and Ni–Nb, similar irradiation experiments were carried out at 843 K for which larger segregation was expected. The results of the analysis are shown in Fig. 7.

4. Discussion

From RIS measurement results of six kinds of Ni binary alloys irradiated under the same irradiation conditions described above, we want to evaluate the

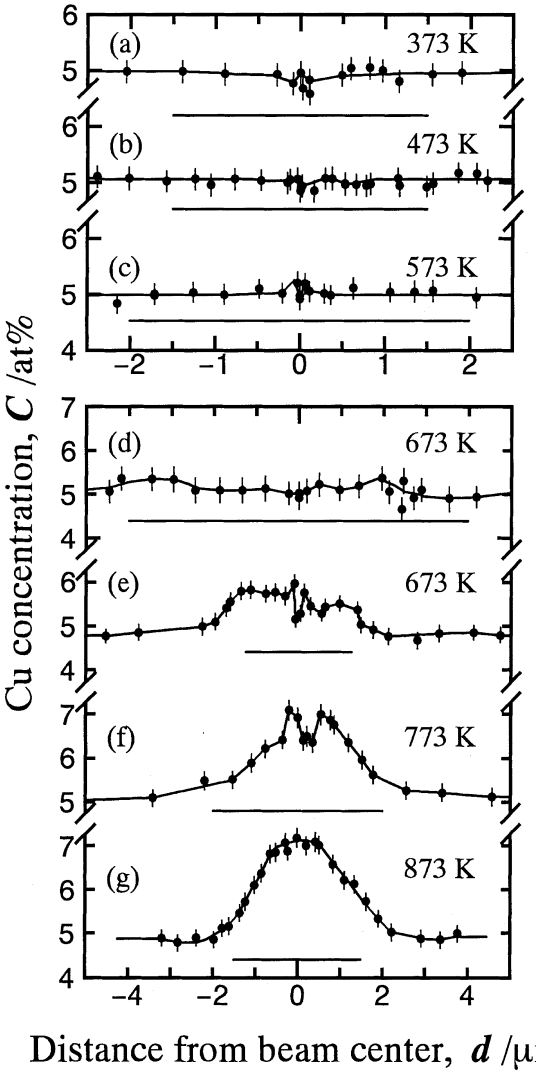

Fig. 2. Cu concentration against the distance from beam center. (a), (b), (c), (d), (e) and (f) corresponds to the micrograph in Figs. 1(a), (b), (c), (d), (e) and (f), respectively. Irradiation conditions of (a), (b), (c), (d), (e) and (f) are the same as Figs. 1(a), (b), (c), (d), (e) and (f), respectively. The irradiation condition in (g), where did not include a grain boundary, is 1.25×10^{24} e^-/m^2 s for 600 s at 873 K.

strength of RIS. RIS happens by the flow of solute atoms and solvent atoms with the flow of excess point defects introduced by irradiation. Since excess vacancies and interstitials flow in the same direction, we estimate the strength of RIS by the flow of point defects instead of each contribution. It is considered that in the case of the experimental conditions used here, there are mainly three flows of point defects: flow from the center caused by the gradients set up by the focused beam, flow to the grain boundary, and flow to the thin foil layer surface.

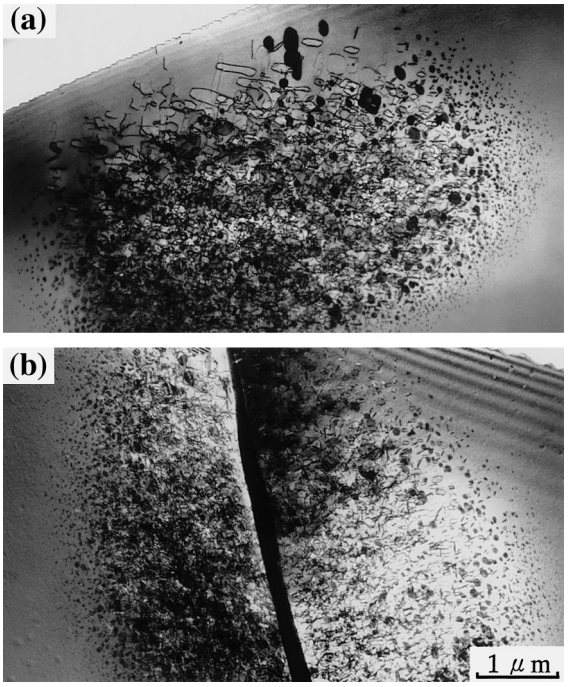

Fig. 3. Electron micrographs of areas (a) without and (b) with a grain boundary in Ni–Mn. Irradiation conditions of both are 5.4×10^{23} e^-/m^2 s for 732 s at 773 K. A grain boundary existed across the beam center in (b).

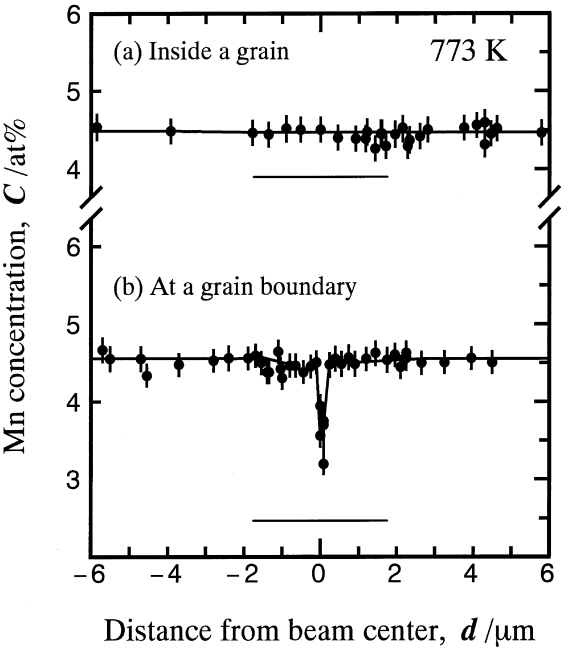

Fig. 4. Mn concentration profiles of the areas shown in Figs. 3(a) and (b). Irradiation conditions are the same as Figs. 3(a) and (b), respectively.

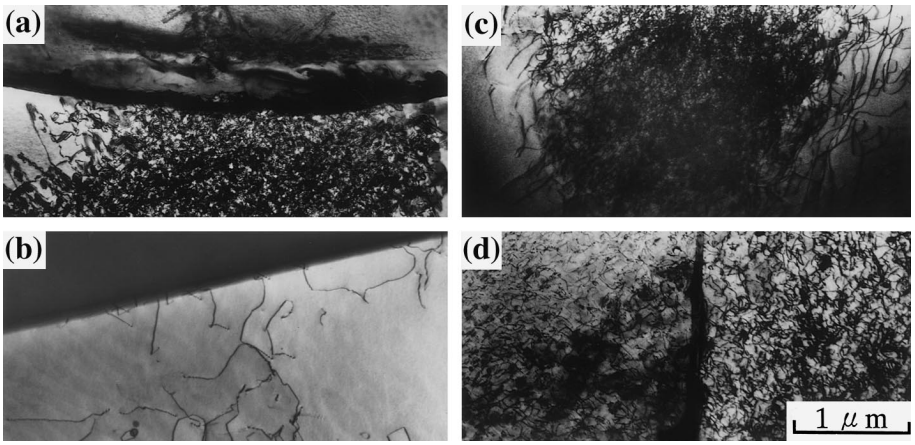

Fig. 5. Electron micrographs of: (a) Ni–Si; (b) Ni–Co; (c) Ni–Pd; and (d) Ni–Nb alloys irradiated with 2 MeV electrons with the same irradiation condition, which is 5.4×10^{23} e^-/m^2 s for 732 s at 773 K. A grain boundary existed across the beam center in each sample.

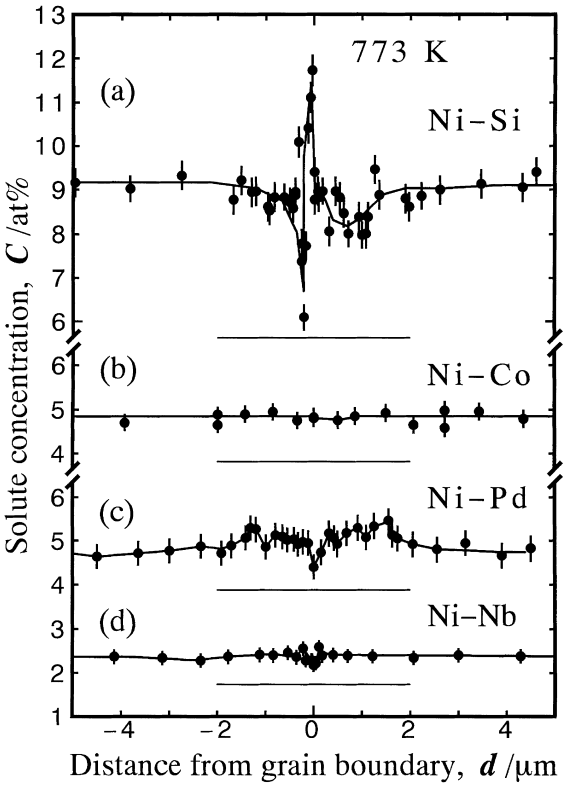

Fig. 6. Solute concentration profiles of the areas corresponding to Figs. 5(a)–(d).

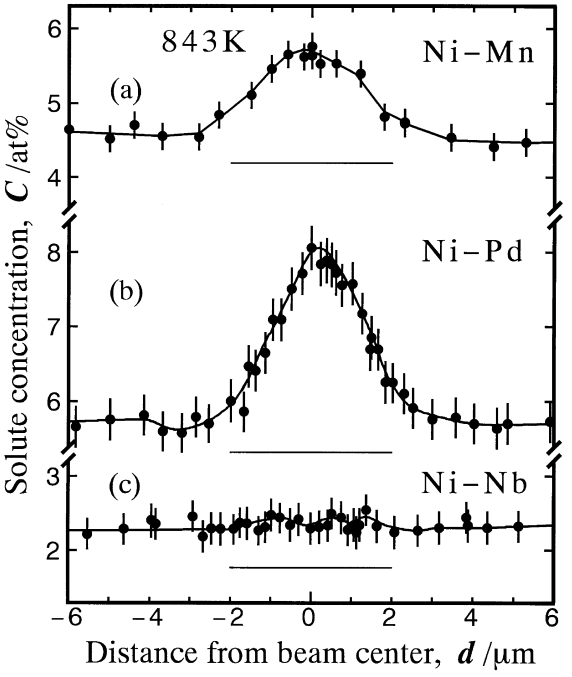

Fig. 7. Solute concentration profiles in: (a) Ni–Mn; (b) Ni–Pd and (c) Ni–Nb alloys irradiated with 2 MeV electrons with the same irradiation condition, which is 5.4×10^{23} e^-/m^2 s for 732 s at 843 K. Irradiated areas did not include a grain boundary.

Segregation to surface hardly affects EDX measured value in plane, since the value is a through-thickness integration. Therefore, the EDX measured values of lateral segregation obtained in this experiment seem to be caused by the other two kinds of flows of point defects. For example, the increase of the solute concentration in an irradiated area with no grain boundary in Figs. 7(a) and (b) is thought to be caused by the flow of point defects due to the radial gradients set up by the focused beam. This is referred to as inverse segregation, since solutes segregate opposite in direction to the flow of point defects. Also the decrease of Mn around the

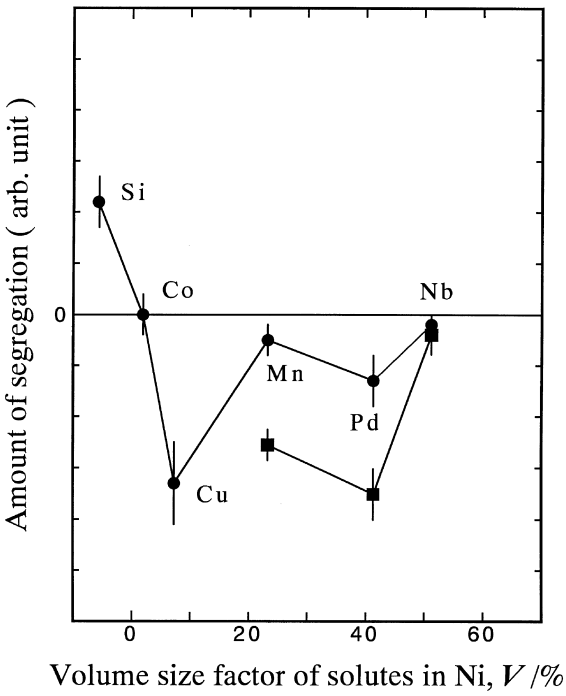

Fig. 8. Amount of RIS at 773 K (full circle) and 843 K (full square) against the volume size factor of the solute atom in Ni binary alloys.

grain boundary in Fig. 4(b) is thought to be caused by the flow of the point defects to the grain boundary. In these cases, the amount of segregation was simply estimated by the area above or below the initial solute concentration, respectively. In other cases, before such a calculation the grain boundary induced segregation very near a grain boundary was separated from the beam gradient segregation by the interpolation around a grain boundary.

The amount of segregation obtained above was divided by the initial solute concentration. Then, it is plotted against the volume size factor [7] of the solute atom in Fig. 8, where normal segregation shows positive. As the volume size factor increases up to about 10%, the amount of segregation decreases. However, as the size increases further, the amount of segregation increases. This result shows that the amount of segregation is not simply related to the size factor [8].

This result is not caused by the pinning effect of dislocations, because only few dislocations are observed at 843 K. In the case of this experiment, the main diffusion process available to solute atoms is the interstitialcy and the vacancy mechanism. The former mechanism leads to normal segregation and the latter to inverse segregation. There are two possibilities for the increase of the amount of segregation in oversized Mn, Pd and Nb in Fig. 8; the decrease of inverse segregation or the increase of normal segregation. The interaction between solute atoms and interstitials is closely related to the density of the interstitial dislocation loops. In Ni–Mn, Ni–Pd, and Ni–Nb in this experiment, the dislocation loop density was larger than that in Ni–Cu in Figs. 1(f), 3(b), 5(c) and (d). Therefore, the interaction between solute atoms and interstitials may increase for the oversized solute atoms such as Mn, Pd and Nb. Consequently, we consider that the increase of the amount of segregation in oversized solutes is caused by the increase of normal segregation due to the interaction between solute atoms and interstitials. From this experiment, it is not possible to discuss the origin of the result of Fig. 8, furthermore.

Acknowledgements

The authors are grateful to Professors H. Fujita and H. Mori, Messrs. K. Yoshida, M. Komatsu and T. Sakata for their help in operating the high voltage electron microscope and the analytical electron microscope.

References

[1] H. Wiedersich, P.R. Okamoto, N.Q. Lam, J. Nucl. Mater. 83 (1979) 98.
[2] T. Ezawa, E. Wakai, R. Oshima, Def. Diff. Forum 95–98 (1993) 252.
[3] T. Hashimoto, Y. Isobe, N. Shigenaka, J. Nucl. Mater. 225 (1995) 108.
[4] T.R. Allen, J.T. Busby, G.S. Was, E.A. Kenik, J. Nucl. Mater. 255 (1998) 44.
[5] T. Ezawa, E. Wakai, Ultramicroscopy 39 (1991) 187.
[6] G. Cliff, G.W. Lorimer, J. Micros. 103 (1975) 203.
[7] H.W. King, J. Mater. Sci. 1 (1996) 79.
[8] L. Kornblit, A. Ignatiev, J. Nucl. Mater. 126 (1984) 77.